Wearable hollow microneedle sensing patches for the transdermal electrochemical monitoring of glucose

Wearable Hollow Microneedle Sensing Patches for the Transdermal Electrochemical Monitoring of Glucose

Marc Parrilla,[a,b,*] Usanee Detamornrat,[c] Juan Domínguez-Robles,[c] Ryan F. Donnelly,[c,*] Karolien De Wael[a,b,*]

[a] A-Sense Lab, Department of Bioscience Engineering, University of Antwerp, Groenenborgerlaan 171, 2020 Antwerp, Belgium.

[b] NANOlab Center of Excellence, University of Antwerp, Groenenborgerlaan 171, 2020, Antwerp, Belgium

[c] School of Pharmacy, Medical Biology Centre, Queen's University Belfast, 97 Lisburn Road, Belfast BT9 7BL, United Kingdom.

ABSTRACT

According to the World Health Organization, about 422 million people worldwide have diabetes, with 1.5 million deaths directly attributed each year. Therefore, there is still a need to effectively monitor glucose in diabetic patients for proper management. Recently, wearable patches based on microneedle (MN) sensors provide minimally invasive analysis of glucose through the interstitial fluid (ISF) while exhibiting excellent correlation with blood glucose. Despite many advances in wearable electrochemical sensors, long-term stability and continuous monitoring remain unsolved challenges. Herein, we present a highly stable electrochemical biosensor based on a redox mediator bilayer consisting of Prussian blue and iron-nickel hexacyanoferrate to increase the long-term stability of the readout coupled with a hollow MN array as a sampling unit for ISF uptake. First, the enzymatic biosensor is developed by using affordable screen-printed electrodes (SPE) and optimized for long-term stability fitting the physiological range of glucose in ISF (i.e. 2.5 to 22.5 mM). In parallel, the MN array is assessed for minimally invasive piercing of the skin. Subsequently, the biosensor is integrated with the MN array leaving a microfluidic spacer that works as the electrochemical cell. Interestingly, a microfluidic channel connects the cell with an external syringe to actively and rapidly withdraw ISF toward the cell. Finally, the robust MN sensing patch is characterized during *in vitro* and *ex vivo* tests. Overall, affordable wearable MN-based patches for the continuous monitoring of glucose in ISF are providing an advent in wearable devices for rapid and life-threatening decision-making processes.

1. Introduction

Wearable devices for health monitoring are currently a revolutionary technology whose mission is to improve life quality, provide body control, and importantly decrease health risks [1–3]. Moreover, a decrease in the healthcare burden and expenditure are foreseen due to early diagnostics, decentralized therapeutic monitoring, and autonomous medication [4].

Still, diabetes is one of the most life-threatening conditions worldwide, being attributed to more than 1.5 million death each year [5]. It is thus clear that a technology that can assist or prevent this medical condition would be valuable to society [6]. The glucometer has been the principal tool for diabetic patients as it allows for tracking their glucose level and accordingly adjusting the optimal level when necessary through insulin injections. Hence, death and side effects from hyper- or hypoglycemia can be avoided. However, the holy grail for glucose sensing is still to be discovered, and therefore, much research in this direction is being performed.

Traditionally, electrochemical glucose sensors have been the gold standard in portable glucose analysis, which is the core technology of the commercially successful glucometer [7]. In the last decade, minimally-invasive monitoring has been approached by many research groups to provide a device that avoids the cumbersome fingerpick that is needed for glucose blood analysis [8–10]. Mainly, sweat and interstitial fluid (ISF) have been targeted as non-invasive matrices by wearable electrochemical sensors which can provide continuous on-body information [7]. In this direction, an in-dwelling subcutaneous device based on a needle (ca. 5 mm) reached commercial success (e.g. Abbott Freestyle libre 3 and Dexcom G6) for continuous glucose monitoring in diabetic patients [11]. However, the needles are still quite long for a painless insertion.

Many developments have been reported for the monitoring of glucose in sweat through epidermal patches [12], textiles [13], or wristbands [14]. Despite some reports on sweat to blood glucose correlation [15,16], it is still unclear whether the sweat glucose levels reflect the metabolic status of the wearer. Besides, the extraction of sweat can be also cumbersome when dealing with diabetic patients and might rely on integrated iontophoretic systems [17].

ISF is of particular interest as it correlates with the glucose levels of blood due to its proximity to blood capillaries which allows a fast diffusion from blood to ISF [18,19]. Besides, ISF can be found in the dermis, below the epidermis which is thus widely available through the skin. Therefore, ISF is a more valuable candidate for wearable glucose monitoring. However, a

suitable element is needed to pierce the stratum corneum of the skin and reach the epidermis and dermis layer for proper ISF sensing. Currently, microneedles (MNs) are used to penetrate and reach ISF [20]. MNs have been employed for drug delivery, ISF extraction, and ISF analysis [21–23]. Another option to avoid piercing the skin is the use of reverse iontophoresis to extract ISF [24]. As the latter technique might produce skin irritation, MN devices are currently the most promising choice to reach ISF.

MNs for sensing applications have been mainly reported in two different ways: (i) use the MNs arrays for ISF extraction which can later perform the analysis *in situ* or send the sample to a laboratory; or (ii) utilize a MNs patch previously functionalized with materials with sensing capabilities. For MN-based electrochemical sensing, mainly five strategies have been described: (i) use of solid MNs coated [25] or sputtered [26] with the appropriate materials; (ii) use of hollow microneedles (HMNs) to embed miniaturized sensors by either a conductive material filling [27], the insertion of a micron-sized wire [28] or even the introduction of the whole miniaturized sensor [29]; and last but not least (iii) the use of a HMNs array connected to an electrochemical cell at the back of the patch for extraction and subsequent analysis of the ISF [30]. The latter strategy utilizes a conventional screen-printed electrode (SPE) coupled to a HMN array, hence, simplifying the functionalization of the MN sensor and potentially decreasing the cost.

Herein, we report a HMNs-based array (HMN) coupled with an electrochemical biosensor based on a highly stable redox mediator bilayer for glucose monitoring in ISF. First, the electrochemical biosensor is optimized for the proper analysis of glucose in ISF levels (from normal to diabetic ranges). The biosensor consists of a SPE modified with glucose oxidase (GOx) and Prussian blue (PB)/nickel hexacyanoferrate (NiHCF) system to increase the stability of the redox mediator layer. Besides, a diffusion-limited layer of Nafion is deposited on the working electrode to expand the linearity of the biosensor to mM levels needed for diabetes monitoring (**Fig. 1A**). In parallel, the HMN array is properly assessed for an easy piercing of the skin (**Fig. 1B**). Subsequently, the biosensor is attached to the back of the HMN array leaving a microfluidic cell (**Fig. 1C**). Finally, the HMN sensing array is coupled to a syringe by means of microfluidic tubing (**Fig. 1D**). This design is essential to have fast ISF extraction and analysis of glucose, as solely diffusion of glucose to the SPE leads to a long-time operation. Thereafter, the HMN sensing is evaluated in *in vitro* tests in an aqueous solution and by piercing the HMN array in foam to simulate the dermis layer. Finally, the HMN sensing patch is interrogated under *ex vivo* tests using porcine skin to emulate the piercing capability of the patch along with the extraction ability of the design. Overall, this work combines a highly stable glucose biosensor with a suitable ISF extraction setup for wearable glucose monitoring in diabetic patients. Interestingly, the wearable platform exhibits the

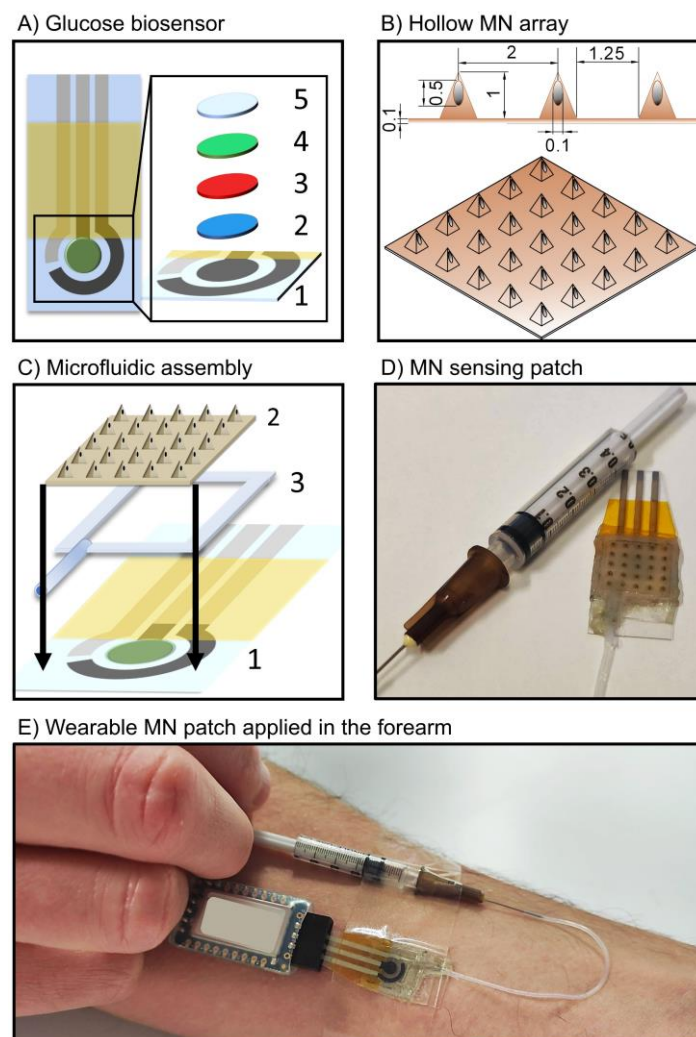potential to be applied in the determination of other key biomarkers for health control (**Fig. 1E**).

Fig. 1. Wearable MN sensing patch for electrochemical glucose monitoring in ISF. A) Glucose biosensor based on a (1) carbon screen-printed electrode with a deposited redox mediator bilayer of (2) Prussian blue and (3) nickel hexacyanoferrate using (4) glucose oxidase enzymatic layer and (5) a Nafion diffusion-limited layer. B) Design and dimensions (in mm) of the HMN array (5 x 5 HMNs) for easy piercing of the skin and ISF extraction. C) Integration of the (1) biosensor with the (2) HMN array leading to a (3) microfluidic cell in between. D) Image of the HMN sensing patch connected to a syringe for active ISF withdrawal. E) Image of the wearable MN sensing patch on a human arm.

2. Experimental section

2.1. Preparation of the MN sensing patch

First, screen-printed electrodes based on carbon working and counter electrodes with a Ag/AgCl pseudo reference electrode were manufactured in-house (see details in

supplementary material). SPEs is the platform where the biosensor and MN sensing patch were built. **Fig. 1A** shows the functionalization of the (1) carbon working electrode in the SPE with a redox mediator bilayer consisting of (2) PB and (3) NiHCF, (4) enzymatic layer based on GOx, (5) and a diffusion-limited layer based on Nafion polymer. Further details on the deposition and characterisation by scanning electron microscopy (SEM) and attenuated total reflectance – Fourier transform infrared (ATR-FTIR) of each layer are described in the supplementary material. The HMN array was designed by computer-aided design (CAD) and fabricated on polyether ether ketone (PEEK) sheets with laser micromachining with specific dimensions to ensure an easy piercing of the skin (**Fig. 1B**). The MN has a pyramidal shape with 1 mm height and 0.75 mm width, a pitch of 2 mm between MNs, which ensures facile penetration with minimal force. The assembly of the MN sensing patch was attained by the introduction of a polyester spacer coated with an adhesive transfer tape that glues the HMN array onto the biosensor, leaving a microfluidic cell between the MN array and the biosensor (**Fig. 1C**). A microfluidic tube was connected to one open side of the spacer. The electrochemical cell had a size of 6 mm x 6.5 mm x 0.674 mm leading to a volume of 26.3 µL. The current thickness of the cell was limited by the external diameter of the microfluidic tubing and the size of the SPE. However, thinner microfluidic cells can be developed by adapting the connector which would account for less ISF volume. **Fig. 1D** shows an image of the MN sensing patch connected to a syringe for active pumping of the ISF.

2.2. *in vitro* evaluation

The analytical performance of the biosensor was performed in PBS 20 mM at pH 7.4 and artificial ISF at pH 7.4. See specific recipes in the supplementary material. Amperometric measurements were carried out by applying -0.1V (vs Ag/AgCl electrode) during 60 s in 100 µL of PBS or artificial ISF. The current obtained at the end of the curve is used for building the calibration curves. The selectivity of the biosensor was assessed by interrogating the biosensor with the interfering species which are glycine (Gly), phenylalanine (Phe), tyrosine (Tyr), caffeine (Caf), ascorbic acid (AA), uric acid (UA), paracetamol (Par), and in the presence of glucose and interfering molecules. The stability experiments were carried out in a closed compartment with the biosensor or MN biosensor immersed in a beaker to avoid evaporation during long-time measurements. Temperature influence was evaluated using a temperature-controlled bath (33±1°C) [31] where the beaker or the biosensor is immersed. The electroanalytical performance of the MN biosensing patch was evaluated by drop-casting 100 µL of artificial ISF on the MN array and pumping in the solution with a syringe to fill in the microfluidic cell. Once, the electrochemical cell is filled with solution the amperometric curve were launched.

2.3. ex vivo evaluation

The analytical performance of the MN sensing patch was assessed after piercing the wearable patch on abdominal porcine skin. Previous to the insertion, fatty tissue from the porcine skin was removed employing a scalpel until a thin skin layer was obtained. The thickness of the skin is measured using a caliper until it reached 500 ±100 μm. To effectively remove the fatty tissue, the porcine skin (20 × 30 mm tissue) was frozen which facilitates the removal of the fatty tissue below the abdominal area. For the penetration of the porcine skin, the skin was positioned on top of 8 layers of Parafilm. Subsequently, the MN sensing patch was pushed with the thumb into the skin for effective piercing. To evaluate the withdrawal capabilities of the HMNs and accordingly the analytical capabilities of the patch, ISF solutions of different concentrations were deposited on the backside of the skin. Subsequently, the ISF was withdrawn to the microfluidic cell for amperometric interrogation by pumping with the syringe.

3. Results and discussion

3.1. Design and characterization of the HMN array

HMNs have attracted much attention for their applications in drug delivery and monitoring [32]. Interestingly, PEEK has proven to be a biocompatible and bioinert material as well as highly resistant to mechanical action [33,34]. In this work, the morphology of the HMN array fabricated with PEEK was first evaluated by using a digital microscope (**Fig. 2A** and **2B** and **S1**). Specifically, **Table S1** shows the dimension parameters measured with the optical microscope. Although these results showed some deviations from the CAD original model, the error could be attributed to the used laser micromachining technique. The percentages of these deviations (N=3) for the MNs body were 1% (tip-to-tip interspacing), 6.8% (hole diameter on MN body), 3.2 % (needle height), and 2.0% (needle width). Only the thickness of the baseplate of the MN array showed a higher percentage of deviation (17%).

To evaluate HMNs insertion, the Parafilm M® insertion model [35] and full-thickness neonatal porcine skin model [36] were both used for this purpose. **Fig. 2C** displays the percentage of holes created in each Parafilm® layer by the HMNs. Indeed, HMNs were able to penetrate up to five layers (625 μm) (**Fig. S2**), since > 80% of holes were created in this fifth layer. Moreover, the results showed that 62.5% of the total needle height was successfully inserted. These results are similar to those found by Larrañeta *et al.*, where 11 x 11 hydrogel-forming microneedle array patches (HFMNs) (900 μm in height) were inserted up to *ca.* 625 μm by using the Parafilm® model and an insertion force of 40 N [35]. The exerted force of 40 N is demonstrated to be necessary to pierce the epidermis layer and reach the interstitial fluid in

6

the dermis layer of the skin. Moreover, HMNs were inserted in full-thickness neonatal porcine skin (*ca*. 500 μm of thickness) by using the Texture Analyser and a force of 40 N. HMNs fully penetrated the porcine skin (100% of holes were created) (**Fig. 2E** and **S3**). Finally, the needle height was measured before and after both insertion tests with no significant differences (p >0.05) (**Fig. 2D** and **2F**). Overall, these results indicated that HMNs arrays are sufficiently robust to overcome the elasticity of the skin and enable its penetration.
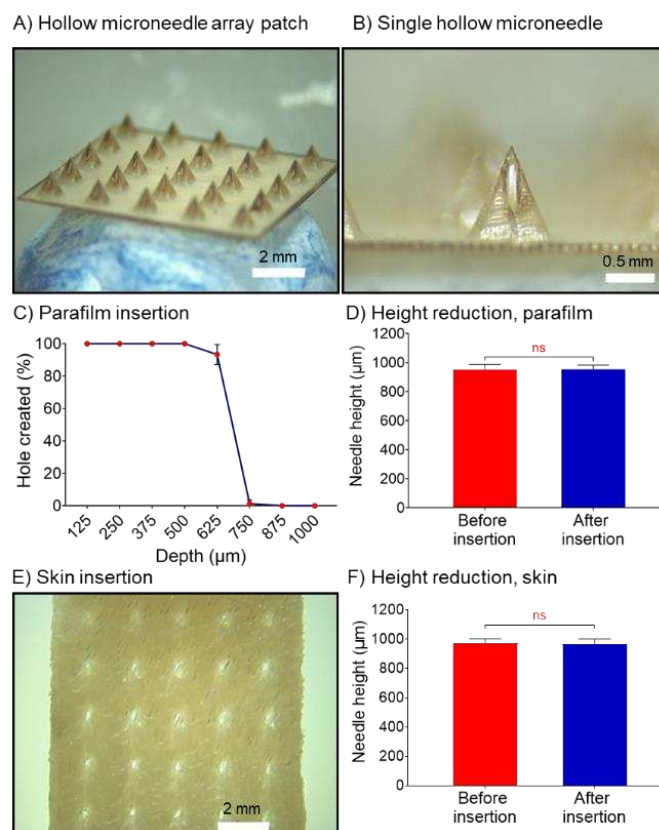

Fig. 2. HMN design and insertion characterization. A) Image of the whole HMN array. B) Image of a single HMN. HMNs penetration during the C) Parafilm insertion test, and D) corresponding height analysis before and after the insertion (N=3). HMNs penetration during the E) porcine skin test, and F) corresponding height analysis before and after the insertion (N=3).

3.2. Highly stable glucose biosensor

The glucose biosensor presented in this work provides two synergic effects to develop suitable glucose biosensors for long-term monitoring. First is the deposition of the NiHCF for the stabilization of the PB mediator layer for hydrogen peroxide reduction [37]. NiHCF has been proven to dramatically increase the stability of the PB as a hydrogen peroxide transducer while

maintaining the catalytic activity even in alkaline conditions [38]. Thereafter, the electrocatalytic bilayer has been integrated into oxidase-based biosensors to improve their stability [39]. In the current glucose biosensor, a preliminary PB layer was deposited (**Fig. S4A**) showing electrocatalytic activity toward hydrogen peroxide formed as a product of the GOx reaction (**Fig. S4B**). Subsequently, the NiHCF as stabilizing layer was electrodeposited by cyclic voltammetry (CV) displaying the characteristic peaks of PB and NiHCF (**Fig. S4C**) [38]. After the deposition of the redox mediator bilayer, its stability was assessed by cycling the potential in PBS pH 7.4 (**Fig. S4D**). The experiment did not show any decrease in the peak current from the deposited mixed nickel-iron hexacyanoferrates proving the high stability of the system at neutral pH conditions. This is important as the biosensor is aimed to be used at physiological pH. Besides, the electrodeposited mediator was characterised by SEM. **Fig. S5** depicts the SEM images of the working electrode at different conditions: (i) graphite (**Fig. S5A**), (ii) PB graphite (**Fig. S5B**), (iii) NiHCF/PB (**Fig. S5C**), and (iv) Nafion/GOx/ NiHCF/PB graphite (**Fig. S5D**). Interestingly, PB particles were deposited (**Fig. S5B**), and serve as the seed layer for the NiHCF layer as can be seen by the increase of the particle size in **Fig. S5C**). Second is the use of a diffusion-limited layer to control the linear range of the biosensor. Typically, electrochemical sensors based on GOx and PB mediator exhibit linearity in the micromolar range [12,17]. However, a higher linear range (i.e. in the millimolar range) is needed to monitor glucose levels in diabetic patients [7]. Therefore, the use of a diffusion-limited layer is essential to reach such levels. In this work, Nafion polymer (**Fig. S5D**), already used for this purpose in electrochemical sensors [40,41], is used taking advantage of three capabilities: (i) limiting the transportation of glucose to the surface of the electrode; (ii) avoiding interferences from negatively charged species; and (iii) decreasing biofouling which is critical in long-term measurements. Finally, the chemical characterisation of the deposited materials at the surface of the working electrode was performed by ATR-FTIR. **Fig. S6** shows the FTIR spectra obtained from the graphite working electrode before and after the modification with the suitable layers. After the deposition of the PB layer, a peak at 2057 cm^{-1} appeared which is the characteristic absorption peak of PB assigned to the stretching vibration of C≡N group in potassium hexacyanoferrate [42]. Moreover, upon the electrodeposition of the NiHCF layer the intensity of the peak increased corresponding to the grown layer of the mediator. This is aligned with the increment of the size of the particles during the electrodeposition. Finally, the deposition of the Nafion layer unravels the typical peaks from Nafion polymer from 1200 to 960 cm^{-1} characteristic from the vibrational bands (i.e. ~1200 cm^{-1} from CF_2 stretching, asymmetric; ~1100 cm^{-1} from CF_2 stretching, symmetric; ~1060 cm^{-1} from S-O stretching, symmetric; ~980 cm^{-1} from C-F stretching; and ~960 cm^{-1} from C-O-C stretching, symmetric) [43].

The analytical performance of the sensor was evaluated at different Nafion layers to show the effect of mass transportation hindrance on the linearity of the biosensor. Hence, the bare biosensor (only enzymatic layer based on chitosan), and the biosensor modified with one to four layers of Nafion were interrogated under increasing concentrations of glucose in PBS (**Fig. S7A-E**). As more Nafion was loaded on the biosensor, a higher concentration of glucose was needed to obtain the analytical readouts. **Fig. S7F** exhibits the corresponding calibration curves showing an increase of the linearity toward the millimolar range of glucose upon increasing layers of Nafion. Expectedly, the slope of the biosensor decreases upon increased Nafion amount as fewer glucose molecules reach the surface of the electrode. Therefore, a compromise between linear range and sensitivity needs to be obtained. It is worth mentioning that the number of Nafion layers might vary during the biosensor fabrication to obtain suitable linearity due to the manual drop-casting method. Hence, a calibration curve should be performed after the deposition of each Nafion layer to check for the desired linearity. On the other hand, depending on the amount of diffusion-limited layers, the biosensor can be tuned toward other target applications (e.g. sweat sensing).

Fig. 3 shows the analytical characterization of the glucose biosensor reaching a linear range from 2.5 to 15 mM suitable for controlling glucose levels in diabetic patients. **Fig. 3A** displays the amperometric curves upon increasing concentrations (N=3 for each concentration). Accordingly, **Fig. 3B** shows the calibration curve exhibiting a slope of -109.7 nA mM^{-1} with a relative standard deviation (RSD) of less than 7% in each of the concentrations. **Fig. 3C** presents a selectivity study performed by interrogating common interfering agents found in biofluids (i.e. glycine, phenylalanine, tyrosine, uric acid, ascorbic acid, caffeine, and paracetamol). **Fig. 3D** manifests that almost no current was generated from the interfering agents. Besides, to verify that the interfering agents do not have any influence on the enzymatic reaction, a mixture of 5 mM glucose with each interferent was carried out. **Fig. S8A** and **S8B** show the amperometric curve of the mixture and the corresponding current values at 60 s. The current intensity did not exhibit a significant difference among interferents showing a RSD of 6.1% (N=8 samples).
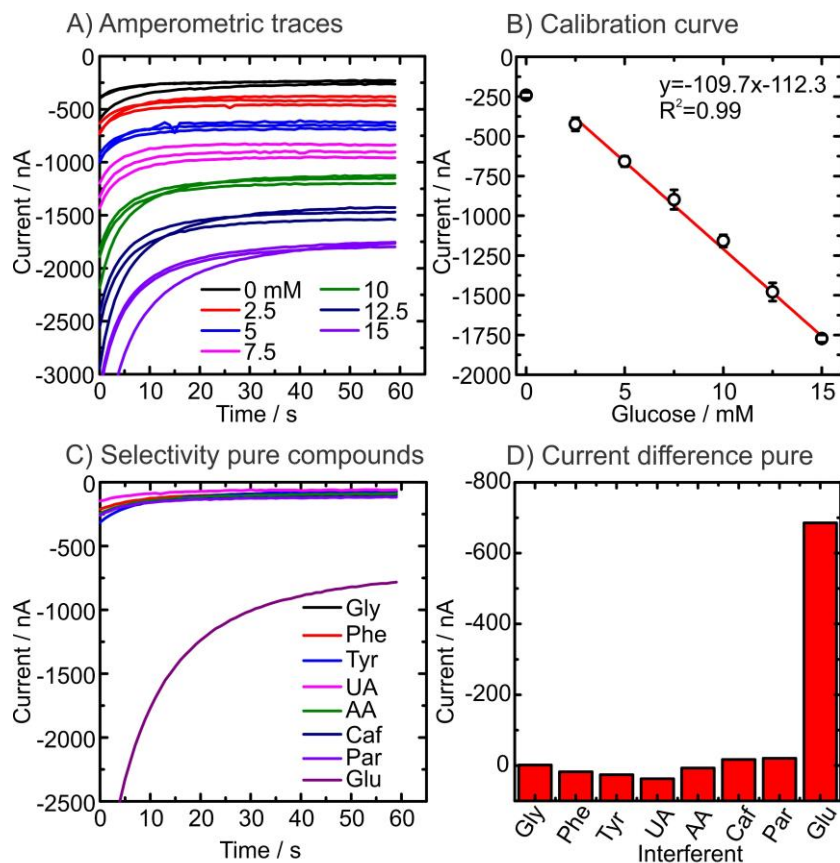
Fig. 3. Analytical performance of the glucose biosensor for the detection of glucose in PBS buffer pH 7.4. A) Consecutive amperometric curves from increasing concentrations of glucose using the same biosensor. B) Corresponding calibration curve. C) Amperometric curves of the selectivity test with common interfering agents at 500 µM: glycine (Gly), phenylalanine (Phe), tyrosine (Tyr), caffeine (Caf), ascorbic acid (AA), uric acid (UA), paracetamol (Par) and glucose (Glu) at 5 mM; and D) respective normalized current difference respect the blank in PBS at 60 s.

An important aspect of the usability of wearable (bio)sensing systems is the expected frequency of measurement to obtain reliable results and the time of analysis of the biosensor. As diabetic patients do not need constant monitoring of glucose and the levels of glucose can be monitored at certain timeframes, amperometric interval monitoring was selected to determine glucose levels. Moreover, the avoidance of continuous amperometric measurements prevents issues in the energy consumption of the entire system. It is important to remark that the interval chosen to perform the interval monitoring influences the sensitivity of the biosensor. Once the sample is in contact with the biosensor, GOx is constantly oxidating glucose to form hydrogen peroxide, which in turn will be reduced by the biosensor only when potential is applied. Therefore, the amperometric signal can increase due to the formation of hydrogen peroxide at the interface which accumulation is governed by the diffusion on the specific electrochemical cell. **Fig. S9A and S9B** show the influence of the time on the cathodic

10

signal, amperograms and peak current vs time results. As much waiting time before applying the potential, the higher the signal, reaching a plateau after 30 min. Therefore, it is important to consider the time during the interval monitoring as it will affect the results on the calibration curve. Regarding the time of analysis, 60 s of amperometry was selected as a balance between repeatability and short electrochemical analysis.

The stability of the readout of wearable electrochemical biosensors is currently one of the bottlenecks that limit their use in real scenarios. In contrast to physical sensors, electrochemical sensors can lose their analytical performance in less time of usability. Traditionally, biosensors can lose performance due to three factors: (i) the degradation of the biorecognition element which in this case is GOx; (ii) the biofouling due to protein adsorption, and (iii) the degradation of the redox mediator layer. The first two factors are tackled as fortunately GOx has demonstrated to be highly stable in combination with BSA and a thick Nafion layer avoids long-term biofouling due to the hydrophilic nature of the polymer, respectively. Consequently, addressing the stability of the redox mediator layer is the missing factor. In this work, the electrochemical deposition of a NiHCF stabilizes the PB layer while maintaining its electrocatalytic feature on hydrogen peroxide [38,39]. **Fig. 4** exhibits the long-term stability of the glucose biosensor during interval monitoring. **Fig. 4A** shows the amperometric curves during more than 14 h of the biosensor immersed in a beaker of 5 mM glucose in PBS pH 7.4 at 22 °C (inset showing a single amperogram). The current output presented a RSD of 6.5% exhibiting high stability of the biosensor (**Fig. 4B**). The same experiment was performed at 33°C (mean temperature of the skin [31]) to evaluate the electrochemical stability in such conditions to emulate the real application. **Fig. 4C** and **4D** display the dynamic curves and the current at 60 s, respectively, during the interval monitoring for more than 12h. Importantly, the redox mediator layer needed 1 h to obtain a stable readout, thereafter showing a RSD of 2.5% among all measurements. To show the high stability of the redox mediator bilayer, continuous amperometry was also assessed (**Fig. S10A**) exhibiting less than 2% in RSD for all data points.
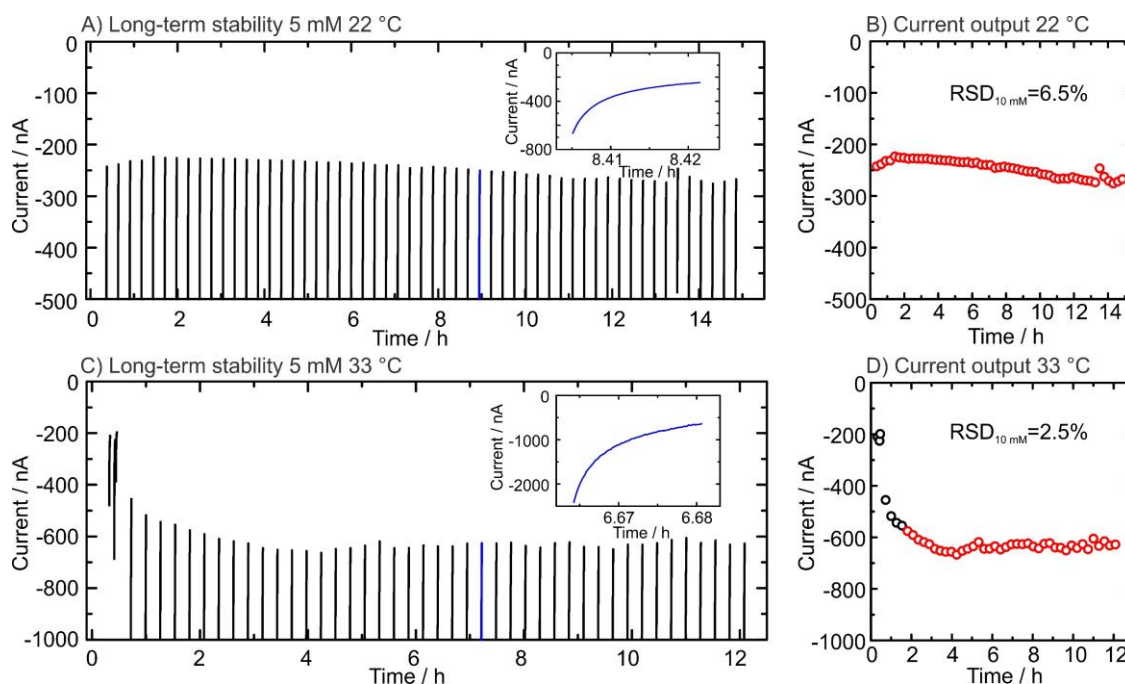
Fig. 4. Long-term stability of the electrochemical signal during interval monitoring. A) Amperograms during more than 14h at 22 °C (inset showing a single dynamic trace), and B) corresponding current at 60 s. C) Amperograms during more than 12h at 33 °C (inset showing a single dynamic trace), and D) corresponding current at 60 s. All measurements were performed in a 5 mL beaker using 5 mM glucose in PBS pH 7.4 by launching the amperometric curve every 15 min.

Temperature plays an important role in enzymatic biosensors due to the dependence on the catalytic activity of the enzymes with temperature. As all analytical characterization of the biosensor was performed at room temperature (i.e. 21-22°C), a calibration curve was also assessed at 33°C. **Fig. S11A** and **S11B** display the dynamic traces of a new biosensor upon increasing glucose concentration (0-15 mM) at 21°C and 33°C, respectively. Accordingly, **Fig. S11C** presents the calibration curve at the aforementioned temperatures exhibiting 1.6-fold higher sensitivity at 33°C. In consequence, it is essential to consider temperature as an influential factor in the electrochemical readout. The incorporation of a temperature sensor is thus paramount for accurate measurements in a future device [12].

3.3. Integration into a MN sensing patch

After the full characterization of the highly-stable biosensor, the integration with the MN array was carried out. First, the passive diffusion of the analytes through the HMN was evaluated. The arrangement consisted of attaching the MN array onto the biosensor leaving a spacer as the electrochemical cell. For this preliminary evaluation, no connection to a syringe with the

microfluidic tube was performed (**Fig. S12A**). The aim is to evaluate whether the analytes can freely diffuse towards the surface of the electrode. To facilitate the entrance and complete wettability of the biosensor surface, a filter paper was placed on the electrochemical cell in between the MN array and the biosensor. Paper capillarity enhances the entrance of the solution to the electrochemical cell. First, 10 mM ferricyanide was used on a regular SPE. **Fig. S12B** shows that the diffusion of the target took 2 min to reach the surface of the working electrode. In contrast, the introduction of the paper on the electrode probably increased the electronic resistance as can be seen in the increment of peak-to-peak distance. A similar test was performed using a bigger molecule (i.e. 10 mM paracetamol) which in this case took 25 min to properly diffuse toward the SPE surface (**Fig. S12C**). It is suggested that diffusion through the MNs holes is occurring although at low rates which might difficult the use of this arrangement for glucose monitoring.

To check the feasibility of the MN sensing patch to monitor glucose, the setup (**Fig. S13A**) was first immersed in a beaker under continuous stirring (i.e. 300 rpm). Upon increasing the concentration of glucose in the beaker from 0 to 15 mM, an increment in the reductive current occurred (**Fig. S13A**). An interval of 15 min was set to allow glucose to diffuse through the HMNs and reach the surface of the biosensor. The MN sensing patch provided linearity from 2.5 – 15 mM with a sensitivity of -64.8 nA mM^{-1} (**Fig. S13B**). Once again, the MN biosensor exhibited excellent stability (i.e. RSD=1.9%) using interval monitoring for 7.5h in a high concentration of glucose (i.e. 10 mM) (**Fig. S13C**) and employing continuous monitoring mode (RSD=6.8%, **Fig. S10B**). Despite the promising results of the arranged MN sensing patch, the electrochemical readout was obtained by employing convection by stirring to allow glucose to reach the biosensor. When only diffusion was imposed, long-time interval times were needed to obtain a current output. Therefore, mass transport only by diffusion-limited the application of this design.

To improve the ISF uptake, the MN sensing patch was slightly modified by introducing a microfluidic tube on one side of the spacer of the electrochemical cell (**Fig. S14A**). Hence, the tube can be connected to a syringe which in turn can provide active extraction of the ISF, and avoid long interval times. A preliminary evaluation of the analytical performance of the biosensor under the microfluidic setup was performed in artificial ISF by adding a 100 μL drop on top of the MN array and pumping the fluid into the electrochemical cell by a syringe (**Video S1**). **Fig. S14B** shows the dynamic traces obtained at increasing concentrations from 2.5 to 22.5 mM (N=3 in each concentration point). The linearity of the biosensor was expanded until 22.5 mM in an attempt to reach high levels of glucose in diabetic patients [44] where immediate action needs to be placed to avoid irreversible metabolic consequences. **Fig. S14C** displays the corresponding calibration curve with a sensitivity of -24.6 nA mM^{-1}. The biosensor

presented a lower sensitivity as it was optimized to fit the linear range up to 22.5 mM and the waiting time after injecting the solution was adjusted to 30 s. Hence, the total operational time is adjusted to 2 min (i.e. 30 s for ISF withdrawal, 30 s for glucose diffusion, and 60 s for the amperometric analysis). Importantly, a RSD of <3% showed excellent repeatability of the MN sensing patch among each concentration. As the ability to monitor glucose fluctuations is paramount in wearable electrochemical devices, a reversibility test was carried out by increasing and decreasing glucose concentration by 5, 10 and 15 mM (**Fig. S14D**). Using all the points at each concentration, a calibration curve was plotted with a slope of -24.2 nA mM^{-1} (**Fig. S14E**). The repeatability for each concentration point was $RSD_{5\ mM}$=5.6 (N=12), $RSD_{10\ mM}$=5.5 (N=18), and $RSD_{15\ mM}$=5.9 (N=9). As some time was needed to obtain a stable response, the first amperogram after changing the concentration was not used for the calculation.

3.4. In vitro characterization of the MN sensing patch under the microfluidic setup

The next step was to assess the analytical performance of the MN sensing patch inserted in a soft material (i.e. foam) to evaluate the withdrawal capability of the system. Hence, the MN patch was inserted into a foam which was subsequently soaked with artificial ISF (**Fig. 5A**). To evaluate the analytical capability, the syringe was used to pump the sample solution toward the electrochemical cell. After filling the cell, a 30 s waiting time was set before launching the amperometric measurement. **Fig. 5B** displays the dynamic traces upon increasing concentrations of glucose (i.e. from 2.5 to 22.5 mM). **Fig. 5C** presents the calibration curve exhibiting a slope of -35.1 nA mM^{-1}. Excellent repeatability was obtained among each glucose concentration (i.e. RSD <4%, N=3 for each concentration). A reversibility test was also executed from 5 to 15 mM to evaluate the ability of the system to monitor fluctuations. **Fig. 5D** plots the dynamic traces upon three complete cycles from normal to diabetic levels of glucose, and **Fig. 5E** exhibits the corresponding calibration plot showing a slope of -32.1 nA mM^{-1}. Besides, the repeatability for each concentration point was $RSD_{5\ mM}$=12.1 (N=12), $RSD_{10\ mM}$=3.8 (N=18), and $RSD_{15\ mM}$=6.0 (N=9). Therefore, the MN sensing patch with active sampling shows outstanding analytical performance for the potential analysis of ISF.
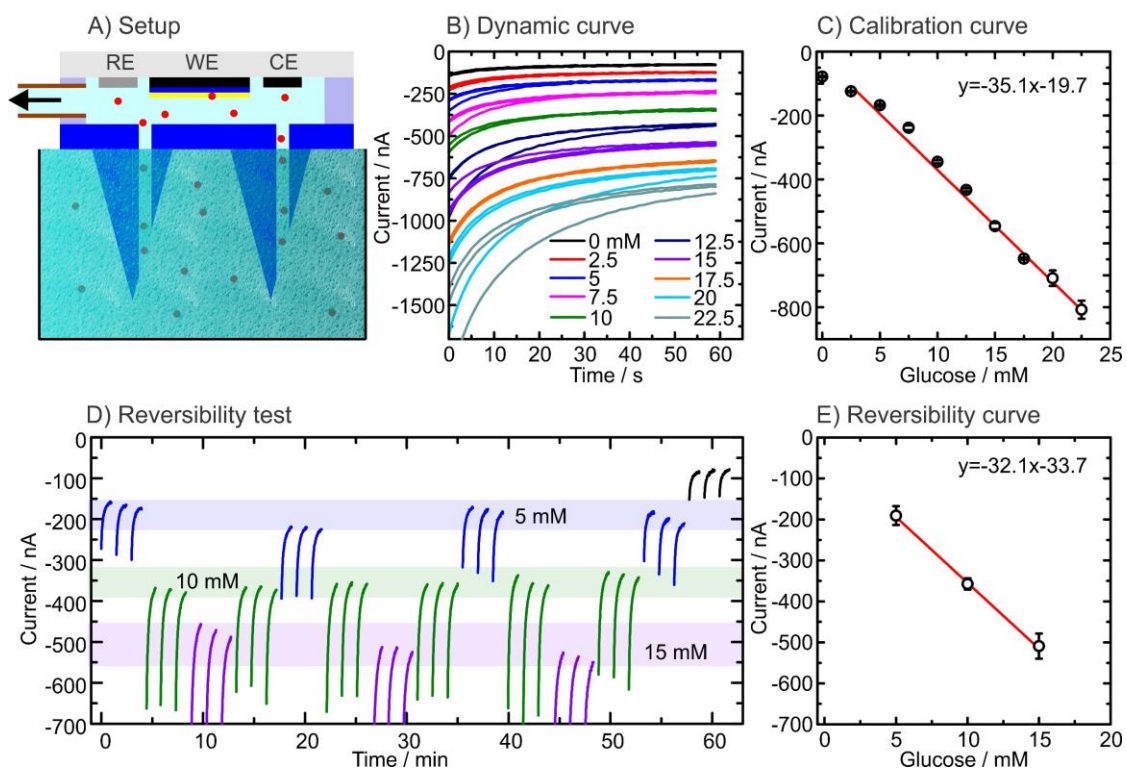
Fig. 5. *In vitro* analytical performance of the MN sensing patch under the microfluidic setup. A) Schematics of the MN sensing patch pierced on foam and soaked with the solution. B) Dynamic traces upon increasing concentrations of glucose (i.e. 2.5 – 22.5 mM) obtained during three consecutive measurements, and C) corresponding calibration curve (N=3). D) Dynamic traces from the reversibility test by changing concentrations of glucose (i.e. 5, 10, and 15 mM), and E) corresponding calibration curve. All experiments were performed in artificial interstitial fluid at pH 7.4. The foam was previously soaked with the sample solution and subsequently introduced onto the electrochemical cell by pumping with the syringe. CE=counter electrode, RE=reference electrode, WE=working electrode.

3.5. ex vivo evaluation of the MN sensing patch.

The ability to pierce the skin and provide ISF withdrawal is the key feature to evaluating the feasibility of the sensing device to be applied in real scenarios. Several works have recently reported the extraction of ISF with MNs, showing the value of ISF as a potential mirror of the physiologic and metabolic status of the body [45,46]. An early work pioneered the ISF extraction with a glass HMN for external glucose analysis using a conventional glucometer [19]. Thus, the extraction and *in situ* analysis still remained a challenge. To combine sampling and electrochemical analysis, a microfluidic chip with a potentiometric sensor was integrated with a HMN for the detection of potassium [47]. This work presented a preliminary analytical characterization with only *in vitro* assays in solution. Another strategy used a densely-packed silicon-dioxide HMN array that allowed for pump-free uptake of ISF [48]. Similarly, the authors

coupled a glucose biosensor at the backside of the MNs array. Nonetheless, the work did not test the device under piercing conditions. Accordingly, it is essential to test the MNs devices in simulated environments such as porcine skin to evaluate the feasibility of such wearable devices.

Considering the promising results by piercing the MN sensing patch in foam, porcine skin was subsequently employed to test the penetration and withdrawal ability. Abdominal porcine skin (500±100 µm thickness) was used for the *ex vivo* experiments (**Fig. S15A**). The piercing of the skin by the MN sensing patch was carried out by placing the skin over 8 layers of Parafilm (skin previously cleaned with PBS pH 7.4), adding on top of the skin the MN sensing patch, and pushing with the thumb towards the skin (**Fig. S15B**). After applying the force with the thumb, the MN sensing patch was reversed visualizing the backside of the penetrated skin (**Fig. 6A** and **S15C**). The images showed that the HMN array successfully penetrates the skin as the tip of the MNs was observed. Moreover, **Video S2** shows the ability to pump solution throughout the pierced skin. Thereafter, the MN sensing patch with the pierced skin was placed backward again into a small cell filled with the proper artificial ISF (**Fig. S15D**) for electrochemical testing. **Fig. 6B** displays the schematics of the setup with the HMN pierced through the porcine skin and allowing the holes to be in contact with the artificial ISF. After the application of the pumping force by the syringe, the MN sensing patch was able to withdraw the sample solution into the microfluidic cell for proper electrochemical analysis (**Video S3**). **Fig. 6C** displays the dynamic traces obtained upon increasing concentrations of glucose (i.e. from 2.5 to 22.5 mM) and **Fig. 6D** presents the corresponding calibration curve exhibiting a slope of -26.1 nA mM^{-1}. The difference in sensitivity could be attributed to the manual deposition (i.e. drop-casting) of the diffusion-limited membrane which can hinder its sensitivity (as previously shown in **Fig. S7**). Indeed, the *ex vivo* calibration curve exhibited less sensitivity than in the *in vitro* test (**Fig. 5C** in foam), but a similar sensitivity than in the solution test (**Fig. S14C**), meaning that there is not any effect by the pierced material and the variation is originated due to the manual manufacturing process. Finally, the MN sensing patch exhibited exceptional reproducibility among each glucose concentration (i.e. RSD <3.5%, N=3 for each concentration point). Therefore, the action of piercing the skin, which implies applying force to the MN sensing patch, did not damage or decrease the analytical performance of the system demonstrating the high robustness and endurance of the wearable MN sensing device. After performing all the electrochemical assays, the experimental setup was unmounted showing the holes of the pierced skin (**Fig. S15E**). Overall, the HMN array proved the capability to pierce real skin and the microfluidic setup confirmed the ability to withdraw solution after skin penetration. Most importantly, the integrated electrochemical glucose biosensor withstands the applied force needed for the piercing of the skin showing an outstanding analytical

performance to monitor glucose at normal and diabetic levels in ISF for a reliable decision-making process.
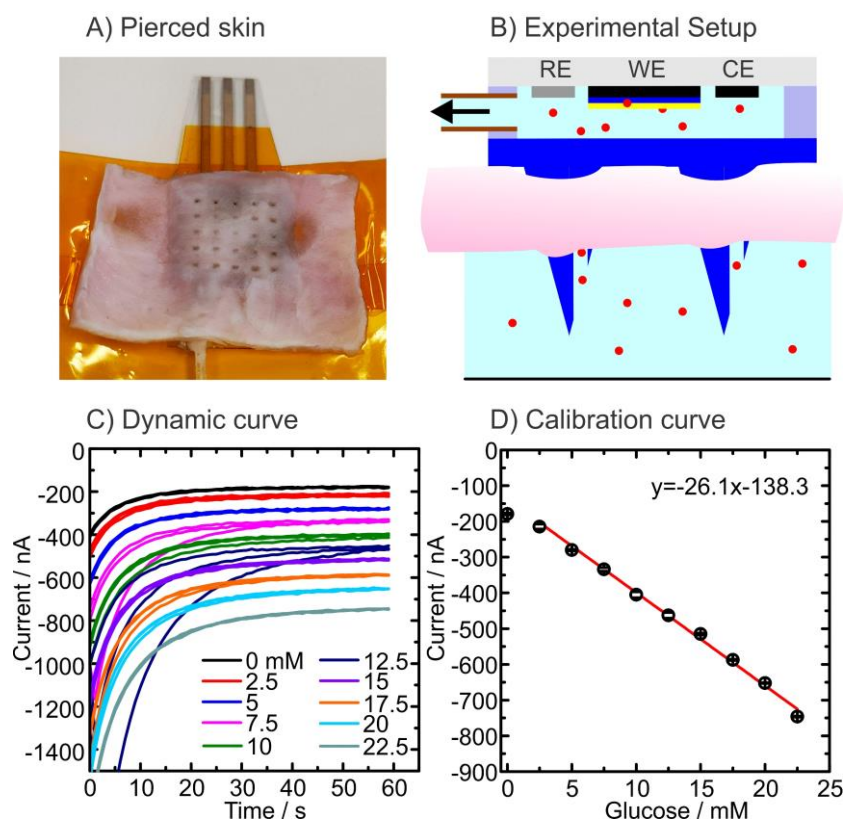

Fig. 6. *Ex vivo* analytical characterization of the MN sensing patch. A) Image of the backside of the pierced porcine skin with the MN sensing patch. B) Schematics of the experimental setup that used the MN sensing patch on pierced porcine skin. C) Dynamic curve obtained from increasing concentrations of glucose, and D) corresponding calibration curve from 2.5 mM to 22.5 mM. All experiments were performed with artificial interstitial fluid at pH 7.4. The microfluidic cell is filled with the solution by pumping with a syringe, and thereafter, amperometry is launched after a 30 s waiting time.

4. Conclusions

In this manuscript, we have first demonstrated the high stability of an electrochemical glucose biosensor by employing a redox mediator bilayer for long-term monitoring coupled with a diffusion-limited layer to be used in wearable electrochemical sensors. Second, we provided a HMN array able to easily pierce the skin and allow ISF withdrawal. Thereafter, the integration of the HMN array on the biosensor to realize a microfluidic MN sensing patch proved the ability to sample ISF by easy pumping with a syringe and *in situ* monitoring glucose. Excellent analytical capabilities were presented fitting the suitable linear range for diabetic patients with

exceptional reversibility performance to monitor glucose fluctuations during potential metabolic events. The reliability of the MN sensing patch has been demonstrated in *in vitro* and *ex vivo* assays using porcine skin. The robustness of the microfluidic patch that allows for the proper piercing of the skin shows promises to use the wearable platform for multiple biomarkers analysis by simply switching the biosensor. Overall, this manuscript demonstrates the feasibility of the integration of highly stable electrochemical biosensors to monitor glucose from normal to diabetic levels with HMNs arrays for ISF extraction, paving the way for an affordable MN sensing patch for painless diabetes management.

Credit author statement

Marc Parrilla: designing methodology, analytical characterization of the electrochemical sensor, and writing the manuscript. **Usanee Detamornrat** and **Juan Domínguez-Robles**: designing the HMN array, designing experiments, characterization of the HMN arrays, and writing the manuscript. **Karolien De Wael** and **Ryan F. Donnelly**: revision of the manuscript and supervision. The manuscript was written through the contributions of all authors. All authors have approved the final version of the manuscript.

Declaration of competing interest

The authors declare that they have no known competing financial interests or personal relationships that could have appeared to influence the work reported in this paper.

Appendix A. Supplementary data

Supplementary data to this article can be found online at https://doi.org/10.1016/j.talanta.2022.XXX

Supplementary Material: Details of the experimental section, electrochemical characterization of the biosensor and the MN sensing patch, and images of the ex vivo test.

Video S1: MN sensing patch working principle

Video S2: Fluid extraction through pierced skin

Video S3: Setup for ex vivo tests.

References

[1]   H. Wang, Y. Zhang, X. Liang, Y. Zhang, Smart Fibers and Textiles for Personal Health Management, ACS Nano. 15 (2021) 12497–12508. https://doi.org/10.1021/acsnano.1c06230.

[2]   Y. Lin, M. Bariya, A. Javey, Wearable Biosensors for Body Computing, Adv. Funct. Mater. (2021) 10.1002/adfm.202008087. https://doi.org/10.1002/adfm.202008087.

[3]   M. Parrilla, K. De Wael, Wearable Self-Powered Electrochemical Devices for Continuous Health Management, Adv. Funct. Mater. 31 (2021) 2107042. https://doi.org/10.1002/adfm.202107042.

[4]   H. Teymourian, M. Parrilla, J.R. Sempionatto, N.F. Montiel, A. Barfidokht, R. Van Echelpoel, K. De Wael, J. Wang, Wearable Electrochemical Sensors for the Monitoring and Screening of Drugs, ACS Sensors. 5 (2020) 2679−2700. https://doi.org/10.1021/acssensors.0c01318.

[5]   World Health Organization, https://www.who.int/health-topics/diabetes#tab=tab_1, Access 07/01/2022. (n.d.).

[6]   T.M. Dall, W. Yang, K. Gillespie, M. Mocarski, E. Byrne, I. Cintina, K. Beronja, A.P. Semilla, W. Iacobucci, P.F. Hogan, The economic burden of elevated blood glucose levels in 2017: Diagnosed and undiagnosed diabetes, gestational diabetes mellitus, and prediabetes, Diabetes Care. 42 (2019) 1661–1668. https://doi.org/10.2337/dc18-1226.

[7]   H. Teymourian, A. Barfidokht, J. Wang, Electrochemical glucose sensors in diabetes management: An updated review (2010-2020), Chem. Soc. Rev. 49 (2020) 7671–7709. https://doi.org/10.1039/d0cs00304b.

[8]   H. Lee, Y.J. Hong, S. Baik, T. Hyeon, D.H. Kim, Enzyme-Based Glucose Sensor: From Invasive to Wearable Device, Adv. Healthc. Mater. 7 (2018) 1701150.

https://doi.org/10.1002/adhm.201701150.

[9] J. Kim, A.S. Campbell, J. Wang, Wearable non-invasive epidermal glucose sensors: A review, Talanta. 177 (2018) 163–170. https://doi.org/10.1016/j.talanta.2017.08.077.

[10] J. Zhang, J. Xu, J. Lim, J.K. Nolan, H. Lee, C.H. Lee, Wearable Glucose Monitoring and Implantable Drug Delivery Systems for Diabetes Management, Adv. Healthc. Mater. 10 (2021) 2100194. https://doi.org/10.1002/adhm.202100194.

[11] U. Hoss, E.S. Budiman, Factory-Calibrated Continuous Glucose Sensors: The Science Behind the Technology, Diabetes Technol. Ther. 19 (2017) S-44-S-50. https://doi.org/10.1089/dia.2017.0025.

[12] A. Wiorek, M. Parrilla, M. Cuartero, G.A. Crespo, Epidermal Patch with Glucose Biosensor: pH and Temperature Correction toward More Accurate Sweat Analysis during Sport Practice, Anal. Chem. 92 (2020) 10153–10161. https://doi.org/10.1021/acs.analchem.0c02211.

[13] Y. Zhao, Q. Zhai, D. Dong, T. An, S. Gong, Q. Shi, W. Cheng, Highly Stretchable and Strain-Insensitive Fiber-Based Wearable Electrochemical Biosensor to Monitor Glucose in the Sweat, Anal. Chem. 91 (2019) 6569−6576. https://doi.org/10.1021/acs.analchem.9b00152.

[14] Y. Zhao, B. Wang, H. Hojaiji, Z. Wang, S. Lin, C. Yeung, H. Lin, P. Nguyen, K. Chiu, K. Salahi, X. Cheng, J. Tan, B.A. Cerrillos, S. Emaminejad, A wearable freestanding electrochemical sensing system, Sci. Adv. 6 (2020) eaaz0007. https://doi.org/10.1126/sciadv.aaz0007.

[15] J. Moyer, D. Wilson, I. Finkelshtein, B. Wong, R. Potts, Correlation Between Sweat Glucose and Blood Glucose in Subjects with Diabetes, Diabetes Technol. Ther. 14 (2012) 398–402. https://doi.org/10.1089/dia.2011.0262.

[16] T.D. La Count, A. Jajack, J. Heikenfeld, G.B. Kasting, Modeling Glucose Transport From Systemic Circulation to Sweat, J. Pharm. Sci. 108 (2019) 364–371. https://doi.org/10.1016/j.xphs.2018.09.026.

[17] A.J. Bandodkar, W. Jia, C. Yardimci, X. Wang, J. Ramirez, J. Wang, Tattoo-based noninvasive glucose monitoring: A proof-of-concept study, Anal. Chem. 87 (2015) 394–398. https://doi.org/10.1021/ac504300n.

[18] J. Heikenfeld, A. Jajack, B. Feldman, S.W. Granger, S. Gaitonde, G. Begtrup, B.A. Katchman, Accessing analytes in biofluids for peripheral biochemical monitoring, Nat.

Biotechnol. 37 (2019) 407–419. https://doi.org/10.1038/s41587-019-0040-3.

[19] P.M. Wang, M. Cornwell, M.R. Prausnitz, Minimally invasive extraction of dermal interstitial fluid for glucose monitoring using microneedles., Diabetes Technol. Ther. 7 (2005) 131–41. https://doi.org/10.1089/dia.2005.7.131.

[20] L. Zhao, C. Zhang, J.M. Abu-Ershaid, M. Li, Y. Li, Y. Naser, X. Dai, M.T.A. Abbate, R.F. Donnelly, Smart Responsive Microarray Patches for Transdermal Drug Delivery and Biological Monitoring, Adv. Healthc. Mater. 10 (2021) 2100996. https://doi.org/10.1002/adhm.202100996.

[21] N.F.N. Ahmad, N.N.N. Ghazali, Y.H. Wong, Concept Design of Transdermal Microneedles for Diagnosis and Drug Delivery: A Review, Adv. Eng. Mater. 23 (2021) 2100503. https://doi.org/10.1002/adem.202100503.

[22] J. Yang, H. Zhang, T. Hu, C. Xu, L. Jiang, Y. Shrike Zhang, M. Xie, Recent advances of microneedles used towards stimuli-responsive drug delivery, disease theranostics, and bioinspired applications, Chem. Eng. J. 426 (2021) 130561. https://doi.org/10.1016/j.cej.2021.130561.

[23] H. Teymourian, F. Tehrani, K. Mahato, J. Wang, Lab under the Skin: Microneedle Based Wearable Devices, Adv. Healthc. Mater. 10 (2021) 2002255. https://doi.org/10.1002/adhm.202002255.

[24] E. De la Paz, A. Barfidokht, S. Rios, C. Brown, E. Chao, J. Wang, Extended Noninvasive Glucose Monitoring in the Interstitial Fluid Using an Epidermal Biosensing Patch, Anal. Chem. 93 (2021) 12767–12775. https://doi.org/10.1021/acs.analchem.1c02887.

[25] M. Parrilla, M. Cuartero, S. Padrell, M. Rajabi, N. Roxhed, F. Niklaus, G.A. Crespo, Wearable All-Solid-State Potentiometric Microneedle Patch for Intradermal Potassium Detection, Anal. Chem. 91 (2019) 1578−1586. https://doi.org/10.1021/acs.analchem.8b04877.

[26] M. Dervisevic, M. Alba, L. Yan, M. Senel, T.R. Gengenbach, B. Prieto-Simon, N.H. Voelcker, Transdermal Electrochemical Monitoring of Glucose via High-Density Silicon Microneedle Array Patch, Adv. Funct. Mater. 32 (2021) 2009850. https://doi.org/10.1002/adfm.202009850.

[27] K.Y. Goud, K. Mahato, H. Teymourian, K. Longardner, I. Litvan, J. Wang, Wearable Electrochemical Microneedle Sensing Platform for Real-Time Continuous Interstitial Fluid Monitoring of Apomorphine: Toward Parkinson Management, Sensors Actuators

B Chem. 354 (2022) 131234. https://doi.org/10.1016/j.snb.2021.131234.

[28] A.M.V. Mohan, J.R. Windmiller, R.K. Mishra, J. Wang, Continuous minimally-invasive alcohol monitoring using microneedle sensor arrays, Biosens. Bioelectron. 91 (2017) 574–579. https://doi.org/10.1016/j.bios.2017.01.016.

[29] F. Ribet, G. Stemme, N. Roxhed, Real-time intradermal continuous glucose monitoring using a minimally invasive microneedle-based system, Biomed. Microdevices. 20 (2018). https://doi.org/10.1007/s10544-018-0349-6.

[30] X. Li, X. Huang, J. Mo, H. Wang, Q. Huang, C. Yang, T. Zhang, H.J. Chen, T. Hang, F. Liu, L. Jiang, Q. Wu, H. Li, N. Hu, X. Xie, A Fully Integrated Closed-Loop System Based on Mesoporous Microneedles-Iontophoresis for Diabetes Treatment, Adv. Sci. 8 (2021) 2100827. https://doi.org/10.1002/advs.202100827.

[31] W. Bierman, The temperature of the skin surface, JAMA - J. Am. Med. Assoc. 106 (1936) 1158–1162. https://doi.org/10.1001/jama.1936.02770140020007.

[32] Á. Cárcamo-Martínez, B. Mallon, J. Domínguez-Robles, L.K. Vora, Q.K. Anjani, R.F. Donnelly, Hollow microneedles: A perspective in biomedical applications, Int. J. Pharm. 599 (2021) 120455. https://doi.org/10.1016/j.ijpharm.2021.120455.

[33] C.H. Rivard, S. Rhalmi, C. Coillard, In vivo biocompatibility testing of peek polymer for a spinal implant system: A study in rabbits, J. Biomed. Mater. Res. 62 (2002) 488–498. https://doi.org/10.1002/jbm.10159.

[34] J.M. Toth, Biocompatibility of PEEK Polymers, 2nd ed., Elsevier Inc., 2019. https://doi.org/10.1016/b978-0-12-812524-3.00008-9.

[35] E. Larrañeta, J. Moore, E.M. Vicente-Pérez, P. González-Vázquez, R. Lutton, A.D. Woolfson, R.F. Donnelly, A proposed model membrane and test method for microneedle insertion studies, Int. J. Pharm. 472 (2014) 65–73. https://doi.org/10.1016/j.ijpharm.2014.05.042.

[36] K. Peng, L.K. Vora, J. Domínguez-Robles, Y.A. Naser, M. Li, E. Larrañeta, R.F. Donnelly, Hydrogel-forming microneedles for rapid and efficient skin deposition of controlled release tip-implants, Mater. Sci. Eng. C. 127 (2021) 112226. https://doi.org/10.1016/j.msec.2021.112226.

[37] Y. Jiang, Y. Yang, L. Shen, J. Ma, H. Ma, N. Zhu, Recent Advances of Prussian Blue-Based Wearable Biosensors for Healthcare, Anal. Chem. 94 (2022) 297–311. https://doi.org/10.1021/acs.analchem.1c04420.

[38]   N.A. Sitnikova, A. V. Borisova, M.A. Komkova, A.A. Karyakin, Superstable advanced hydrogen peroxide transducer based on transition metal hexacyanoferrates, Anal. Chem. 83 (2011) 2359–2363. https://doi.org/10.1021/ac1033352.

[39]   E. V. Karpova, E.E. Karyakina, A.A. Karyakin, Accessing Stability of Oxidase-Based Biosensors via Stabilizing the Advanced H 2 O 2 Transducer, J. Electrochem. Soc. 164 (2017) B3056–B3058. https://doi.org/10.1149/2.0091705jes.

[40]   D. Chen, C. Wang, W. Chen, Y. Chen, J.X.J. Zhang, PVDF-Nafion nanomembranes coated microneedles for in vivo transcutaneous implantable glucose sensing, Biosens. Bioelectron. 74 (2015) 1047–1052. https://doi.org/10.1016/j.bios.2015.07.036.

[41]   M. Parrilla, R. Cánovas, F.J. Andrade, Paper-based enzymatic electrode with enhanced potentiometric response for monitoring glucose in biological fluids, Biosens. Bioelectron. 90 (2017) 110–116. https://doi.org/10.1016/j.bios.2016.11.034.

[42]   A.M. Farah, C. Billing, C.W. Dikio, A.N. Dibofori-Orji, O.O. Oyedeji, D. Wankasi, F.M. Mtunzi, E.D. Dikio, Synthesis of prussian blue and its electrochemical detection of hydrogen peroxide based on cetyltrimethylammonium bromide (CTAB) modified glassy carbon electrode, Int. J. Electrochem. Sci. 8 (2013) 12132–12146.

[43]   Z. Liang, W. Chen, J. Liu, S. Wang, Z. Zhou, W. Li, G. Sun, Q. Xin, FT-IR study of the microstructure of Nafion® membrane, J. Memb. Sci. 233 (2004) 39–44. https://doi.org/10.1016/j.memsci.2003.12.008.

[44]   J.P. Bantle, W. Thomas, Glucose measurement in patients with diabetes mellitus with dermal interstitial fluid., J. Lab. Clin. Med. 130 (1997) 436–441. https://doi.org/10.1016/S0022-2143(97)90044-5.

[45]   P.P. Samant, M.M. Niedzwiecki, N. Raviele, V. Tran, J. Mena-Lapaix, D.I. Walker, E.I. Felner, D.P. Jones, G.W. Miller, M.R. Prausnitz, Sampling interstitial fluid from human skin using a microneedle patch, Sci. Transl. Med. 12 (2020) eaaw0285. https://doi.org/10.1126/SCITRANSLMED.AAW0285.

[46]   C. Kolluru, R. Gupta, Q. Jiang, M. Williams, H. Gholami Derami, S. Cao, R.K. Noel, S. Singamaneni, M.R. Prausnitz, Plasmonic Paper Microneedle Patch for On-Patch Detection of Molecules in Dermal Interstitial Fluid, ACS Sensors. 4 (2019) 1569–1576. https://doi.org/10.1021/acssensors.9b00258.

[47]   P.R. Miller, X. Xiao, I. Brener, D.B. Burckel, R. Narayan, R. Polsky, Microneedle-based transdermal sensor for on-chip potentiometric determination of K+, Adv.

Healthc. Mater. 3 (2014) 876–881. https://doi.org/10.1002/adhm.201300541.

[48] L.M. Strambini, A. Longo, S. Scarano, T. Prescimone, I. Palchetti, M. Minunni, D. Giannessi, G. Barillaro, Self-powered microneedle-based biosensors for pain-free high-accuracy measurement of glycaemia in interstitial fluid, Biosens. Bioelectron. 66 (2015) 162–168. https://doi.org/10.1016/j.bios.2014.11.010.